Labile Complexes of the $[RuTp(pn)]^+$ (Tp = Tripyrazolylborate, pn = $Ph_2PCH_2CH_2NMe_2$) Fragment Including the Dinitrogen Ligand[1]

Gregor Trimmel,[†] Christian Slugovc,[†] Petra Wiede,[‡] Kurt Mereiter,[‡] Valentin N. Sapunov,[†,§] Roland Schmid,[†] and Karl Kirchner*[,†]

Institute of Inorganic Chemistry and Institute of Mineralogy, Crystallography, and Structural Chemistry, Technical University of Vienna, Getreidemarkt 9, A-1060 Vienna, Austria

Received September 12, 1996[⊗]

The $[TpRu(pn)]^+$ fragment (Tp = tripyrazolyl, pn = $Ph_2PCH_2CH_2NMe_2$), featuring a strong σ acceptor and a weak π donor, forms reversible complexes with a variety of σ donor ligands L including N_2 which appears to be more strongly bonded than even CH_3CN. X-ray crystal structures of the complexes with L = H_2O, acetone, CO, N_2, and vinylidene are included (adding to that for L = CH_3CN from former work), as well as a comparative MO study on the bonding nature of L. The sequence of complex stabilities of $[TpRu(pn)L]^+$ is $CF_3SO_3^-$ < acetone ≈ H_2O < CH_3CN < N_2 < CO < vinylidene as suggested from EHMO calculations and crystallographic data as well as qualitative experimental results. Despite the notable stability of $[TpRu(pn)(\eta^1\text{-}N_2)]^+$, the N−N bond length is 1.097(5) Å, exactly that in free N_2. Our analysis suggests that the insensitivity of the N−N bond essentially originates from the counterbalance of π bond weakening (through back-donation) and σ bond strengthening (through reducing the antibonding character of the σ^* ($2\sigma_u$) MO in molecular dinitrogen.

Introduction

In Part 2 of this series[1] we have investigated the coordination−chemical properties of the $[RuTp(tmeda)]^+$ fragment (Tp = tripyrazolylborate and tmeda = $Me_2NCH_2CH_2NMe_2$). The studies were motivated by the desire to systematically learn about the conditions that may favor the generation of highly labile or eventually coordinatively unsaturated metal complexes featuring probable or potential intermediate products in catalytic cycles. In the case of the $CpRu^+$ and Cp^*Ru^+ fragments combined with bulky co-ligands, the creation of five-coordinate ruthenium(II) complexes was feasible[2−5] due to the fact that all d AOs of Ru are mixing, making the d(π) orbitals bonding in character. In the $[RuTp(tmeda)]^+$ fragment, on the other hand, the vacant coordination site is appreciably π-basic since the d(π) AOs of ruthenium are virtually not engaged in holding the square pyramid of $[RuTp(tmeda)]^+$ together. It has been found that the stability of $[RuTp(tmeda)L]^+$ is increasing with L in the order THF < $CF_3SO_3^-$ < acetone < CH_3CN ≈ dmf which is not the order of their σ-donor strengths as expressed by their donor numbers (DN).[1] Therefore, $\pi-\pi$ and $\pi-$p interactions are expected to be the major contributors to the Ru−L bonding.

To analyze the underlying interactions further we continue in the present work our studies on the $TpRu^+$ fragment chemistry by switching over from N,N to the mixed-donor chelating N−P bidentate co-ligand $Ph_2PCH_2CH_2NMe_2$ (pn) and investigate the products of chloride abstraction from RuTp(pn)Cl (**1**). In particular we are interested in seeing whether the different electronegativities of P and N are large enough to provoke changes in the reactivity patterns. For some time there has been interest in using so-called hemilabile ligands as a supporting factor toward creating undercoordinated species.[4,6,7] Incidentally, it should be mentioned that mixed N−P bidentates can be ligated to the $TpRu^+$ fragment more easily than to $CpRu^+$. Furthermore, the presence of phosphorus is very helpful, allowing speciation studies of labile complexes in solution to be done through ^{31}P NMR spectroscopy.

Experimental Section

General Information. All reactions were performed under an inert atmosphere of purified argon by using Schlenk techniques and/or a glovebox unless otherwise noted. All chemicals were standard reagent grade and used without further purification. The solvents were purified and dried according to standard procedures and stored over 4 Å molecular sieves.[8] The deuterated solvents were purchased from Aldrich and dried over 4 Å molecular sieves. RuTp(pn)Cl (**1**) was prepared according to the literature.[9] ^1H, $^{13}C\{^1H\}$, and $^{31}P\{^1H\}$ NMR spectra were recorded on a Bruker AC-250 spectrometer operating at 250.13, 62.86, and 101.26 MHz, respectively, and were referenced to $SiMe_4$ and to H_3PO_4 (85%). Diffuse reflectance FT-IR spectra were recorded on a Mattson RS 2 spectrometer. Microanalyses were done by Microanalytical Laboratories, University of Vienna.

Synthesis. RuTp(pn)(CF_3SO_3) (2). A solution of **1** (200 mg, 0.330 mmol) and $TlCF_3SO_3$ (125 mg, 0.353 mmol) in dry CH_2Cl_2 (5 mL) was stirred for 12 h at room temperature. After removal of the solvent, the residue was redissolved in CH_2Cl_2 and insoluble materials were removed by filtration. On addition of diethyl ether, a yellow precipitate was obtained, which was collected on a glass frit, washed with diethyl ether, and dried under vacuum. Yield: 198 mg (81%). Anal. Calcd

[†] Institute of Inorganic Chemistry.
[‡] Institute of Mineralogy, Crystallography, and Structural Chemistry.
[§] On leave of absence from D. Mendeleyev University of Chemical Technology of Russia, Miusskaja 9, 125047 Moscow, Russia.
[⊗] Abstract published in *Advance ACS Abstracts,* February 15, 1997.

(1) Part 2: Gemel, C.; Wiede, P.; Mereiter, K.; Sapunov, V. N.; Schmid, R.; Kirchner, K. *J. Chem. Soc., Dalton Trans.* **1996**, 4071.
(2) Campion, B. K.; Heyn, R. H.; Tilley, D. D. *J. Chem. Soc., Chem. Commun.* **1988**, 278.
(3) (a) Kirchner, K.; Mauthner, K.; Mereiter, K.; Schmid, R. *J. Chem. Soc., Chem. Commun.* **1993**, 892. (b) Mauthner, K.; Mereiter, K.; Schmid, R.; Kirchner, K. *Inorg. Chim. Acta* **1995**, *236*, 95.
(4) Lindner, E.; Haustein, M.; Mayer, H. A.; Gierling, K.; Fawzi, R.; Steinmann, M. *Organometallics* **1995**, *14*, 2246.
(5) Sutter, J.-P.; James, S. L.; Steenwinkel, P.; Karlen, T.; Grove, D. M.; Veldman, N.; Smeets, W. J. J.; Spek, A. L.; van Koten, G. *Organometallics* **1996**, *15*, 941.
(6) Jeffrey, J. C.; Rauchfuss, T. B. *Inorg. Chem.* **1979**, *18*, 2658.
(7) Werner, H.; Schulz, M.; Windmüller, B. *Organometallics*, **1995**, *14*, 3659.
(8) Perrin, D. D.; Armarego, W. L. F. *Purification of Laboratory Chemicals*, 3rd ed.; Pergamon: New York, 1988.
(9) Gemel, C.; Trimmel, G.; Slugovc, C.; Mereiter, K.; Kremel, S.; Schmid, R.; Kirchner, K. *Organometallics* **1996**, *15*, 3998.

S0020-1669(96)01128-7 CCC: $14.00

for $C_{26}H_{30}BF_3N_7O_3PRuS$: C, 43.34; H, 4.20; N, 13.61. Found: C, 43.64; H, 4.49; N, 13.36. ^{1}H NMR (δ, CD_2Cl_2, 20 °C): 8.36 (d, 1H, J = 1.6 Hz), 7.92 (d, 1H, J = 2.3 Hz), 7.77 (d, 1H, J = 2.3 Hz), 7.68 (d, 1H, J = 2.6 Hz), 7.47 - 7.27 (m, 6H), 7.10 (m, 2H), 6.93 (d, 1H, J = 1.9 Hz), 6.75 (m, 2H), 6.46 (m, 1H), 6.20 (d, 1H, J = 1.9 Hz), 6.01 (dd, 1H, J = 2.3 Hz, J = 1.6 Hz), 5.62 (dd, 1H, J = 2.3 Hz, J = 2.3 Hz), 3.30 (m, 1H), 2.94 (m, 3H), 2.87 (s, 3H), 2.28 (s, 3H). ^{13}C{^{1}H} NMR (δ, CD_2Cl_2, 20 °C): 147.9, 147.0, 144.5 (d, ^3J(PC) = 3.5 Hz), 137.5, 135.9, 135.7, 133.3−128.6 (10 C), 105.9, 105.7, 105.6, 64.7 (d, ^2J(PC) = 6.2 Hz), 53.9, 52.9, 28.4 (d, ^1J(PC) = 23.6 Hz). ^{31}P{^{1}H} NMR (δ, CD_2Cl_2, 20 °C): 67.8.

Formation of $[RuTp(pn)(H_2O)](CF_3SO_3)$ (3). In order to obtain crystals of **2** for X-ray diffraction, a solution of **2** in CH_2Cl_2 was set aside for crystallization by vapor diffusion with diethyl ether. Within 1 day a small amount of pale yellow crystals were formed which, however, turned out to be the water complex **3**, instead of **2**.

Reaction of 2 with H_2O. Formation of $[RuTp(pn)(H_2O)](CF_3SO_3)$ (3). A 5 mm NMR tube was charged with a solution of **2** (30 mg, 0.042 mmol) in CD_2Cl_2 (0.5 mL) and was capped with a septum. H_2O (20 μL, 1.11 mmol) was added, and the sample was transferred to a NMR probe. A ^{31}P{^{1}H} NMR spectrum was immediatly recorded, showing signals at 67.8 and 71.1 ppm due to the presence of **2** and **3**.

$[RuTp(pn)(\eta^1$-acetone)$]CF_3SO_3$ (4). A solution of **1** (200 mg, 0.330 mmol) and $TlCF_3SO_3$ (125 mg, 0.353 mmol) in dry CH_2Cl_2 (5 mL) containing 5% of acetone was stirred for 6 h at room temperature. After that time the solvent was removed in vacuo, and the residue was redissolved in CH_2Cl_2. Insouble materials were removed by filtration. The filtrate was again evaporated to dryness, and the residue was dissolved in 2 mL of acetone. The product was precipitated by slow addition of diethyl ether to yield orange crystals of **5**, which were collected on a glass frit, washed with diethyl ether, and dried under vacuum. Yield: 190 mg (74%). Anal. Calcd for $C_{29}H_{36}BF_3N_7O_4PRuS$: C, 44.74; H, 4.46; N, 12.59. Found: C, 45.03; H, 4.29; N, 12.45. ^{1}H NMR (δ, acetone-d_6, 20 °C): 8.16 (d, 1H, J = 2.2 Hz), 8.13 (d, 1H, J = 2.2 Hz), 7.97 (d, 1H, J = 2.3 Hz), 7.90 (d, 1H, J = 2.4 Hz), 7.42 (m, 6H), 7.20 (m, 2H), 6.93 (m, 2H), 6.72 (d, 1H, J = 2.1 Hz), 6.55−6.50 (m, 2H), 6.09 (m, 1H), 5.83 (m, 1H), 3.58 (m, 2H), 3.38 (m, 2H), 2.87 (s, 3H), 2.36 (s, 3H), 2.09 (s, 6H, free acetone). In CD_2Cl_2 as the solvent, coordinated acetone gives rise to a singlet at 1.55 ppm (6H). ^{13}C{^{1}H} NMR (δ, acetone-d_6, 20 °C): 206.8, 149.6, 146.9, 144.4, 139.7, 138.4, 137.9, 136.9−129.8, 108.3, 108.0, 107.4, 66.1 (d, J(PC) = 5.6 Hz), 53.9, 52.6, 31.3, 28.6 (d, J(PC) = 25.6 Hz). ^{31}P{^{1}H} NMR (δ, acetone-d_6, 20 °C): 69.0. IR (diffuse reflectance, cm^{-1}): 2459 (m, B-H), 1653 (s, C═O).

Reaction of 2 with CH_3CN. Formation of $[RuTp(pn)(CH_3CN)]CF_3SO_3$ (5). A 5 mm NMR tube was charged with a solution of **2** (30 mg, 0.042 mmol) in acetone-d_6 (0.5 mL) and was capped with a septum. CH_3CN (20 μL, 0.487 mmol) was added, and the sample was transferred to a NMR probe. ^{1}H, ^{13}C{^{1}H} and ^{31}P{^{1}H} NMR spectra were immediately recorded, showing the quantitative formation of **5**.[9]

$[RuTp(pn)(CO)]CF_3SO_3$ (6). A solution of **1** (200 mg, 0.330 mmol) in dry THF (5 mL) was treated with $TlCF_3SO_3$ (116 mg, 0.330 mmol) under an CO atmosphere for 3 h at room temperature. The solvent was removed under vacuum and the residue was dissolved in CH_2Cl_2. Insoluble materials were filtered off, and the volume of the filtrate was reduced to about 2 mL. On addition of diethyl ether, an orange precipitate was formed, which was collected on a glass frit, washed with diethyl ether, and dried under vacuum. Yield: 170 mg (69%). Anal. Calcd for $C_{27}H_{30}BF_3N_7O_4PRuS$. C, 43.33; H, 4.04; N, 13.10. Found: C, 43.56; H, 4.12; N, 13.02. ^{1}H NMR (δ, $CDCl_3$, 20 °C): 7.97 (d, 1H, J = 1.4 Hz), 7.80 (d, 1H, J = 1.8 Hz), 7.73 (m, 2H), 7.51−7.34 (m, 6H), 7.15 (m, 2H), 6.80 (m, 3H), 6.65 (m, 1H), 6.43 (m, 1H), 6.07 (m, 1H), 5.93 (m, 1H), 3.35−2.96 (m, 4H, CH_2CH_2), 3.30 (s, 3H, CH_3), 2.27 (s, 3H, CH_3). ^{13}C{^{1}H} NMR (δ, $CDCl_3$, 20 °C): 202.2 (d, J(PC) = 15.8 Hz) 145.9, 144.4, 143.3, 137.9, 137.3, 137.2, 133.4−124.9, 108.0, 107.8, 106.9, 64.6 (d, J(PC) = 4.2 Hz), 57.2, 53.7, 27.3 (d, J(PC) = 30.3 Hz). ^{31}P{^{1}H} NMR (δ, $CDCl_3$, 20 °C): 56.0. IR (diffuse reflectance, cm^{-1}): 2510 (m, B−H), 1980 (s, CO).

$[RuTp(pn)(=C=CHPh)]CF_3SO_3$ (7). A solution of **1** (600 mg, 0.989 mmol) in dry THF (7 mL) was treated with phenylacetylene (0.5 mL) in the presence of $TlCF_3SO_3$ (353mg, 0.990 mmol) for 2 h at room temperature. The solvent was removed under vacuum, and the residue was dissolved in CH_2Cl_2. Insoluble materials were filtered off, and the volume of the filtrate was reduced to about 2 mL. On addition of diethyl ether, a red precipitate was formed, which was collected on a glass frit, washed with diethyl ether, and dried under vacuum. Yield: 698 mg (86%). Anal. Calcd for $C_{34}H_{36}BF_3N_7O_3PRuS$. C, 49.64; H, 4.41; N, 11.92. Found: C, 48.83; H, 4.19; N, 12.09. ^{1}H NMR (δ, CD_2Cl_2, 20 °C): 8.01 (d, 1H, J = 2.3 Hz), 7.88 (m, 2H), 7.80 (d, 1H, J = 2.4 Hz), 7.53−7.33 (m, 6H), 7.20 (m, 2H), 7.02 (m, 3H), 6.72 (m, 4H), 6.51 (m, 2H), 6.44 (m, 1H), 6.10 (m, 1H), 6.04 (m, 1H), 5.04 (d, 1H, J(PH) = 4.0 Hz, C═C*H*—Ph), 3.33−3.02 (m, 4H, CH_2CH_2), 3.11 (s, 3H, CH_3), 2.22 (s, 3H, CH_3). ^{13}C{^{1}H} NMR (δ, CD_2Cl_2, 20 °C): 371.8 (d, J(PC) = 20.1 Hz) 145.9, 144.4, 142.7, 137.7, 137.2, 136.9, 133.2−125.8, 112.6 (d, J_{CP} = 1.6 Hz), 107.3, 107.0, 106.5, 64.4 (d, J(PC) = 4.7 Hz), 58.6, 53.4, 26.4 (d, J(PC) = 30.5 Hz). ^{31}P-{^{1}H} NMR (δ, acetone-d_6, 20 °C): 52.2. IR (diffuse reflectance, cm^{-1}): 2505 (m, B−H), 1655 (s, C═C).

Reaction of 2 with Phenylacetylene. Formation of $[RuTp(pn)(=C=CHPh)]CF_3SO_3$ (7). A 5 mm NMR tube was charged with a solution of **2** (30 mg, 0.042 mmol) in acetone-d_6 (0.5 mL) and was capped with a septum. Phenylacetylene (20 μL, 0.196 mmol) was added, and the sample was transferred to a NMR probe. A ^{31}P{^{1}H} NMR spectrum was immediatly recorded, showing the quantitative formation of **7**.

$[RuTp(pn)(\eta^1$-$N_2)]BPh_4$ (8). A solution of **1** (250 mg, 0.412 mmol) was treated with $NaBPh_4$ (142 mg, 0.415 mmol) in CH_2Cl_2 and was stirred at room temperature for 30 h under a nitrogen atmosphere. Insoluble materials were removed by filtration, and the solution was set aside for crystallization by vapor diffusion with diethyl ether. Within 1 day pale yellow crystals of **8**·CH_2Cl_2 were formed suitable for an X-ray diffraction and elemental analysis. Anal. Calcd for $C_{50}H_{52}B_2Cl_2N_9Ru$. C, 59.84; H, 5.22; N, 12.56. Found: C, 58.37; H, 5.30; N, 12.65. IR (diffuse reflectance, cm^{-1}): 2486 (m, B-H), 2182 (s, N≡N).

X-ray Structure Determination for 3·$^1/_2CH_2Cl_2$, 4, 6, 7·CH_2Cl_2, and 8·CH_2Cl_2. Crystal data and experimental details are given in Table 1. X-ray data for 3·$^1/_2CH_2Cl_2$, 7·CH_2Cl_2, and 8·CH_2Cl_2 were collected on a Philips PW 1100 four-circle diffractometer using graphite-monochromated Mo Kα (λ = 0.710 73 Å) radiation and the $\theta-2\theta$ scan technique. For **4** and **6**, a Siemens Smart CCD area detector diffractometer, graphite-monochromated Mo Kα radiation, a nominal crystal-to-detector distance of 6 cm, and 0.3° ω-scan frames were used. Corrections for Lorentz and polarization effects, for crystal decay, and for absorption were applied. The structures were solved by Patterson or direct methods.[10] All non-hydrogen atoms were refined anisotropically, and hydrogen atoms were included in idealized positions.[11] The structures were refined against F^2. Selected bond distances and angles are given in Table 2.

EHMO Calculations. The extended Hückel molecular orbital calculations were conducted by using the original program developed by Hoffmann and Lipscomb,[12] and modified by Mealli and Proserpio.[13] The atomic parameters used in this study were taken from the CACAO program.

Results and Discussion

Substitutionally Labile Complexes. Chloride abstraction from RuTp(pn)Cl (**1**)[9] using $TlCF_3SO_3$ in CH_2Cl_2 as the solvent gives RuTp(pn)(η^1-OSO_2CF_3) (**2**) as a yellow powder in essentially quantitative yield (Scheme 1). The close similarity between the ^{1}H, ^{13}C{^{1}H} and ^{31}P{^{1}H} solution NMR spectra between **2** and the neutral 18 electron complex **1**[9] advocates against an ionic $[RuTp(pn)]^+CF_3SO_3^-$ composition. Instead, triflate appears to be directly bonded to the metal center thus

(10) Sheldrick, G. M. SHELXS86: Program for the Solution of Crystal Structures. University of Göttingen, Germany, 1986.
(11) Sheldrick, G. M. SHELXL93: Program for Crystal Structure Refinement. University of Göttingen, Germany, 1993.
(12) (a) Hoffman, R.; Lipscomb, W. N. *J. Chem. Phys.* **1962**, *36*, 2179. (b) Hoffman, R.; Lipscomb, W. N. *J. Chem. Phys.* **1962**, *36*, 3489. (c) Hoffman, R. *J. Chem. Phys.* **1963**, *39*,.1397.
(13) Mealli, C.; Proserpio, D. M. *J. Chem. Educ.* **1990**, *67*, 399.

Table 1. Crystallographic Data

	3·$^1/_2CH_2Cl_2$	**4**	**6**	**7**·CH_2Cl_2	**8**·CH_2Cl_2
formula	$C_{26.5}H_{33}BClF_3N_7O_4PRuS$	$C_{29}H_{36}BF_3N_7O_4RuS$	$C_{27}H_{30}BF_3N_7O_4PRuS$	$C_{35}H_{38}BCl_2F_3N_7O_4PRuS$	$C_{50}H_{52}B_2Cl_2N_9PRu$
fw	780.96	778.56	748.49	907.53	1003.57
cryst size, mm	0.33 × 0.33 × 0.44	0.1 × 0.1 ×.0.4	0.32 × 0.35 × 0.41	0.1 × 0.3 × 0.7	0.06 × 0.28 × 0.80
color	yellow	yellow	orange	red	yellow
space group	$P\bar{1}$ (No. 2)	$P2_1/c$ (No. 14)	$P\bar{1}$ (No. 2)	$P\bar{1}$ (No. 2)	$P\bar{1}$ (No. 2)
a, Å	10.031(2)	9.939(2)	13.675(2)	9.938(3)	11.368(3)
b, Å	12.611(2)	12.931(2)	14.352(2)	13.757(5)	13.870(3)
c, Å	13.607(3)	26.281(3)	17.692(3)	16.536(6)	17.115(4)
α, deg	105.63(1)		67.30(1)	66.20(2)	84.25(1)
β, deg	95.51(1)	91.43(1)	88.04(1)	77.62(2)	78.84(1)
γ, deg	101.33(1)		85.50(1)	70.55 (2)	68.92(1)
V, Å^3	1605.0(5)	3376.6(9)	3193.4(8)	1942(1)	2469(1)
Z	2	4	4	2	2
ρ_{calc}, g cm^{-3}	1.616	1.532	1.557	1.552	1.350
T, °C	25	25	25	23	21
μ, cm^{-1} (Mo Kα)	7.49	6.36	6.69	6.96	5.02
abs cor	empirical	empirical	empirical	analytical	empirical
transm factors, min/max	0.95/1.09	0.93/1.07	0.63/0.80	0.85/0.93	0.82/1.19
θ_{max}, deg	25	26.3	27	23.1	24
index ranges	$-11 \le h \le 11$	$-11 \le h \le 12$	$-13 \le h \le 19$	$-10 \le h \le 10$	$-12 \le h \le 12$
	$-14 \le k \le 14$	$0 \le k \le 13$	$-17 \le k \le 20$	$-13 \le k \le 15$	$-15 \le k \le 15$
	$0 \le l \le 16$	$0 \le l \le 32$	$-23 \le l \le 24$	$0 \le l \le 18$	$0 \le l \le 19$
no. of rflns measd	5562	9124	21472	5418	7737
no. of unique rflns	5562	4710	13366	5418	7737
no. of rflns F > 4σ(F)	4886	4066	10578	4424	5285
no. of params	423	424	812	535	601
$R_1(F)$ ($F > 4\sigma(F)$)	0.028	0.043	0.040	0.042	0.050
$R_2(F)$ (all data)	0.036	0.058	0.056	0.058	0.091
w$R_2(F^2)$ (all data)	0.069	0.090	0.100	0.109	0.112
diff Fourier peaks min/max, e Å^{-3}	−0.54/0.43	−0.53/0.44	−0.76/0.51	−0.35/0.36	−0.49/0.51

[a] $R_1 = \sum||F_o| - |F_c||/\sum|F_o|$, $wR_2 = [\sum(w(F_o^2 - F_c^2)^2)/\sum(w(F_o^2)^2)]^{1/2}$.

Table 2. Selected Bond Distances (Å) and Angles (deg) of the $[RuTp(pn)L]^+$ Complexes

	L					
	H_2O	acetone	CH_3CN[a]	N_2	CO	=C=CHPh
Ru−L	2.190(2)	2.104(3)	2.013(2)	1.943(4)	1.853(3)	1.821(5)
Ru−$N_{(trans\ to\ L)}$	2.071(2)	2.075(4)	2.093(2)	2.102(4)	2.175(2)	2.209(4)
Ru−N(pn)	2.220(2)	2.228(4)	2.206(2)	2.205(4)	2.214(3)	2.214(4)
Ru−P	2.274(1)	2.275(1)	2.269(1)	2.286(2)	2.312(1)	2.309(2)
Ru−$N_{(trans\ to\ P)}$	2.168(2)	2.169(3)	2.137(2)	2.141(4)	2.154(3)	2.146(4)
Ru−$N_{(trans\ to\ N(pn))}$	2.065(2)	2.076(4)	2.076(2)	2.090(4)	2.038(3)	2.076(4)
Ru−X−Y (XY = L)		137.1(3)	170.3(2)	174.6(4)	175.1(3)	169.6(4)

[a] Reference 9.

adding to the small number of known ruthenium complexes bearing the η^1-OSO_2CF_3 ligand.[5,14,15] In attempting to get crystals suitable for X-ray studies for direct proof, however, instead of **2**, pale yellow crystals of the aquo complex [RuTp(pn)(H_2O)]CF_3SO_3 (**3**) were obtained. The water obviously originated from the CH_2Cl_2 solution, despite rigorous drying, although in solution the aquo complex could not be detected unless extra H_2O has been added. In fact, the gradual reaction of **2** with H_2O could be followed by $^{31}P\{^1H\}$ NMR experiments. Thus, on admixing H_2O to a solution of **2** in CD_2Cl_2, in addition to the resonance at 67.8 ppm assignable to **2**, a second resonance appeared at 71.7 ppm due to the formation of **3** indicating the equilibrium

$$\underset{\mathbf{2}}{RuTp(pn)(\eta^1\text{-}OSO_2CF_3)} + H_2O \rightleftharpoons \underset{\mathbf{3}}{[RuTp(pn)(H_2O)]^+} + CF_3SO_3^- \quad (1)$$

However, owing to the low solubility of water in CD_2Cl_2, this equilibrium is always largely shifted to the left.

In the presence of small amounts of acetone, chloride abstraction from **1** with $TlCF_3SO_3$ in CH_2Cl_2 (**1** is poorly soluble in neat acetone), the cationic complex [RuTp(pn)(η^1-acetone)]CF_3SO_3 (**4**) is formed in 74% yield (Scheme 1). Similarly, in neat acetone, **2** is quantitativly converted to **4** as monitored by ^1H and $^{31}P\{^1H\}$ NMR spectroscopy. While this complex is air stable in the solid state, slow decomposition takes place in solution. In CD_2Cl_2, **4** and **2** are about equally present as seen from ^1H and $^{31}P\{^1H\}$ NMR spectroscopy data pointing to the equilibrium

$$\underset{\mathbf{4}}{[RuTp(pn)(\eta^1\text{-acetone})]^+} + CF_3SO_3^- \rightleftharpoons \underset{\mathbf{2}}{RuTp(pn)(\eta^1\text{-}OSO_2CF_3)} + \text{acetone} \quad (2)$$

Extra addition of acetone shifts the equilibrium completely to the left. Incidentally, the triflate in **2** is also easily displaced by CH_3CN and CO to form $[RuTp(pn)(CH_3CN)]^+$ (**5**) and $[RuTp(pn)(CO)]^+$ (**6**). Complex **5** has already been described before (as the BPh_4^- salt).[9]

Complexes **1**, **2**, and **4** are excellent precursors for the synthesis of vinylidene complexes as depicted in Scheme 1. The reaction of **1** with phenylacetylene in the presence of $TlCF_3SO_3$ in THF leads, in high yields, to the cationic vinylidene

(14) Kraakman, M. J. A.; de Klerk-Engels, B.; de Lange, P. P. M.; Vrieze, K.; Smeets, W. J. J.; Spek, A. L. *Organometallics* **1992**, *11*, 3774.
(15) Plosser, P. W.; Gallucci, J. C.; Wojcicki, A. *Inorg. Chem.* **1992**, *31*, 2376.

Scheme 1

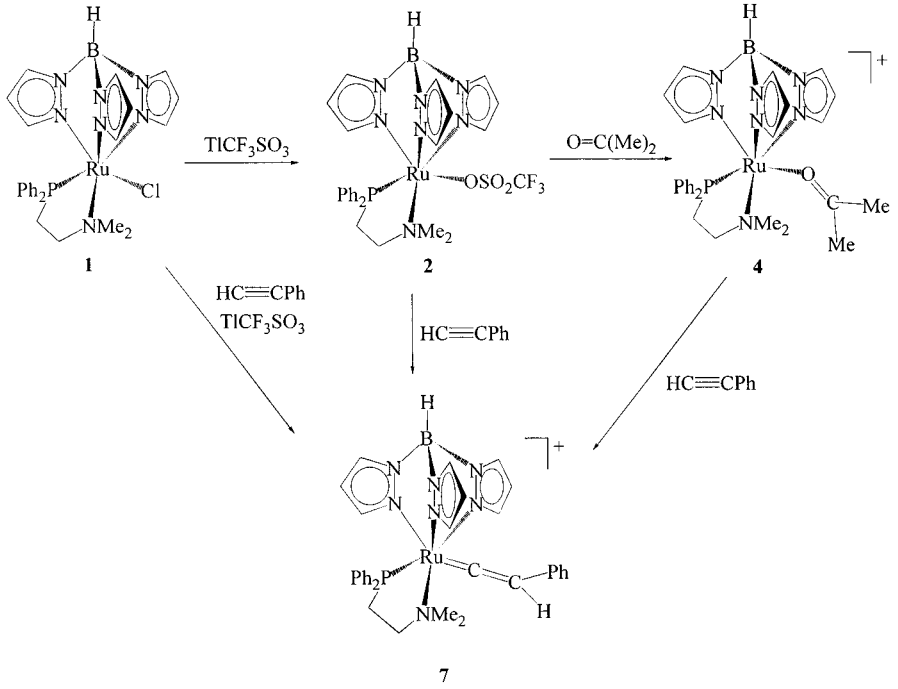

complex $[RuTp(pn)(=C=CHPh)]^+$ (**7**) as an air-stable red solid. Likewise, treatment of either **2** or **4** with phenylacetylene (≤ 1 equiv) in acetone-d_6 affords **7** in nearly quantitative yield as monitored by ^{1}H NMR spectroscopy.

Next we performed chloride abstraction from **1** with $NaBPh_4$ instead of $TlCF_3SO_3$ in CH_2Cl_2 as the solvent. While under an argon atmosphere complete decomposition of the starting material takes place, under nitrogen the cationic complex $[RuTp(pn)(\eta^1\text{-}N_2)]^+$ (**8**) is formed which, by vapor diffusion of diethyl ether, is isolated as pale yellow crystals. In acetone-d_6 as the solvent, **8** is quantitativly converted to **4**, whereas in CD_2Cl_2 several as yet unidentified products are formed.

On the basis of the above reactions, the qualitative trend in ligand strengths may be suggested to be $CF_3SO_3^- < H_2O <$ acetone $< CH_3CN < CO <$ vinylidene, comparable with that found previously for RuTp(tmeda)L[1] as noted in the Introduction. Considering the low concentration of dinitrogen present in solution but nevertheless sufficient to form the dinitrogen complex **8** in the presence of residual water in the solvent CH_2Cl_2, the ligand strength of N_2 is to be viewed as higher than that of water at least.

Characterization of the Various RuTp(pn)L Complexes. The crystal structure of $[RuTp(pn)(H_2O)]CF_3SO_3 \cdot {}^1/_2CH_2Cl_2$ (**3**·$^1/_2CH_2Cl_2$) shows two cationic moieties linked via hydrogen bonds between the water ligands and the $CF_3SO_3^-$ anions, forming a crystallographic centrosymmetric neutral dimeric species (Figure 1). The hydrogen bond O···O distances are 2.828 and 2.966 Å. A closely related neutral dimeric species with crystallographic point symmetry (C_1) and hydrogen bond O···O distances of 2.714−2.802 Å was recently found in $[RuTp(COD)(H_2O)]CF_3SO_3$ (COD = 1,5-cyclooctadiene).[9] The Ru−O(1) distance is 2.190 (2) Å, comparable to that observed in $[RuTp(COD)(H_2O)]CF_3SO_3$, $[RuCp^*(CO)_2(H_2O)]^+$, and $[Ru(HCpz_3)(H_2O)_3]^{2+}$ ($HCpz_3$ = tris(pyrazolylmethane)) being 2.151(4), 2.173(3), and 2.131(1) Å), respectively.[9,16,17] A somewhat longer Ru−O bond distance is found in $[RuCp^*(nbd)(H_2O)]BF_4$ (nbd = norbornadiene) (2.238 (5) Å).[18] The geometry at ruthenium is approximately octahedral. The bite angle of the Tp ligand produces an average N−Ru−N angle of 86.6° only slightly distorted from the right angle.

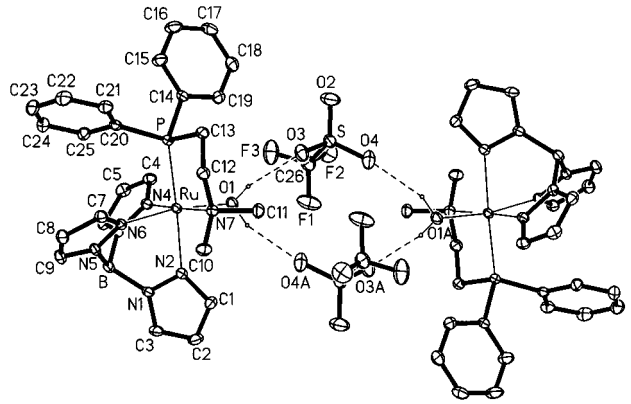

Figure 1. Structural view of $[RuTp(pn)(H_2O)]CF_3SO_3 \cdot CH_2Cl_2$ (**3**·CH_2Cl_2) (CH_2Cl_2 omitted for clarity).

Complex $[RuTp(pn)(\eta^1\text{-acetone})]CF_3SO_3$ (**4**) is characterized as follows. The ^{1}H and $^{13}C\{^1H\}$ NMR spectra in acetone-d_6 exhibit three distinct sets of pyrazol-1-yl resonances pointing to the existence of three types of pyrazol-1-yl rings in a 1:1:1 ratio. The $^{31}P\{^1H\}$ NMR spectrum gives a singlet at 69.0 ppm. In the ^{1}H NMR spectrum the NMe_2 group of the pn ligand displays two singlets at 2.87 (3H) and 2.36 ppm (3H); i.e., the methyl groups are diastereotopic. In the IR spectrum the ν(C=O) band is observed at 1653 cm^{-1}, in line with other ruthenium acetone complexes (Table 3). This value is lower than the frequency of the free ligand appearing at 1710 cm^{-1} consistent with coordination reducing the C=O bond strength. The ν(B−H) vibration is found at 2459 cm^{-1} which is characteristic of terdentate *N*,*N*′,*N*″-bonded Tp. A structural view of **4** is depicted in Figure 2. The acetone molecule is strongly attached to the metal giving a relatively short Ru−O distance of 2.104(3) Å. Some structural data of related

(16) Thiri, A.; Guerchais, L.; Toupet, L.; Lapinte, C. *J. Organomet. Chem.* **1990**, C47.
(17) Llobet, A.; Hodgson, D. J.; Meyer, T. J. *Inorg. Chem.* **1990**, 29, 3760.
(18) Suzuki, H.; Kakigano, T.; Fukui, H.; Tanaka, M.; Moro-oka, Y. *J. Organomet. Chem.* **1994**, *473*, 295.

Table 3. Selected IR Spectroscopic and X-ray Crystallographic Data for the Ruthenium η^1-Acetone Complexes

compound	ν(C═O), cm^{-1}	Ru−O, Å	C═O, Å	∠Ru−C−O, deg	ref
[RuTp(pn)(acetone)]$^+$ (**5**)	1653	2.104(3)	1.237(6)	137.1(3)	this work
[RuTp(tmeda)(acetone)]$^+$	1649	2.103(2)	1.243(4)	136.5(2)	1
Ru(PPh$_3$)$_2$(CO)(SnCl$_3$)Cl(acetone)	1661	2.194(8)	1.238(9)	153.0(5)	19
[Ru{C(═CHPh)OC(O)Me}(PPr$^i_3$)$_2$(CO)(acetone)]$^+$	1680	2.205(6)	1.235(10)	164.7(6)	20
Ru$_2$(μ-O$_2$CEt)$_4$(acetone)$_2$	1684	2.363(5)	1.214(5)	135.1(3)	21

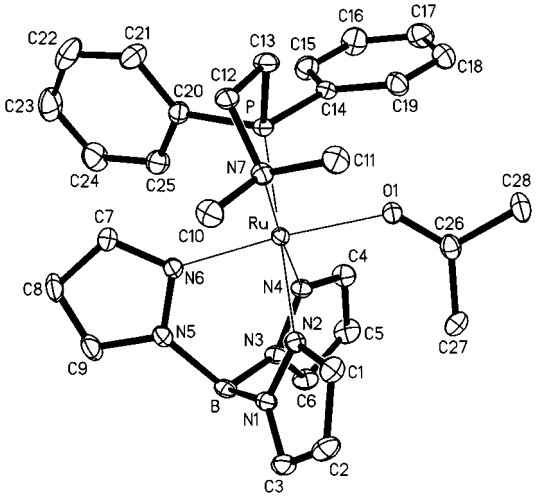

Figure 2. Structural view of [RuTp(pn)(η^1-acetone)]CF_3SO_3 (**4**) ($CF_3SO_3^-$ omitted for clarity).

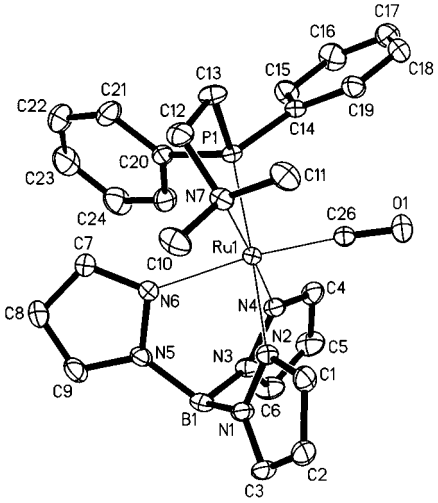

Figure 3. Structural view of [RuTp(pn)(CO)]CF_3SO_3 (**6**) ($CF_3SO_3^-$ omitted for clarity).

complexes are given in Table 3 for comparison purposes. The coordination geometry of **4** is approximately octahedral with all angles at ruthenium between 85 and 95° and between 177 and 178°. There are no structural features pointing to unusual deviations or distortions. The Ru−N(4) and Ru−N(6) distances are 2.076(2) and 2.075(2) Å, respectively, and thus are very similar, while the one *trans* to the phosphorus atom (Ru−N(2)) is significantly longer with 2.169(3) Å. The Ru−N(pn) and Ru−P bond distances are 2.275 (1) and 2.228 (4) Å.

The NMR spectra of **6** exhibits the resonances of Tp and pn in the expected ranges. In the IR spectrum of **6** the ν(CO) absorption is observed at 1980 cm^{-1}. A structural view of **6**, as determined by X-ray crystallography, is shown in Figure 3. The coordination geometry of this complex is approximately octahedral exhibiting bond distances and angles very similar to those of **3**, **4**, and **5**.[9] However, the Ru−N bond distance trans to the CO ligand is significantly longer, being 2.175(2) Å. The coordinated CO is almost linear, being 175.1(3)°.

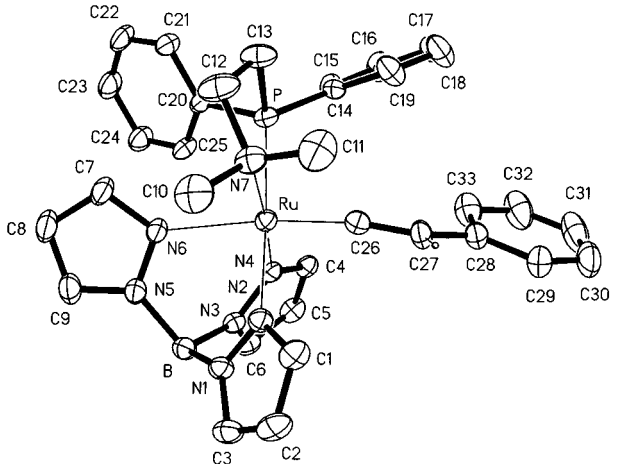

Figure 4. Structural view of [RuTp(pn)(═C═CHPh)]CF_3SO_3·CH_2Cl_2 (**7**·CH_2Cl_2) ($CF_3SO_3^-$ and CH_2Cl_2 omitted for clarity).

Characteristic spectroscopic features of the cationic vinylidene complex [RuTp(pn)(═C═CHPh)]$^+$ (**7**) comprise, in the ^{13}C-{^{1}H} NMR spectrum, a marked low-field resonance at 371.8 ppm (d, J_{CP} = 20.1 Hz) and a signal at 112.6 ppm (d, J_{CP} = 1.6 Hz) assignable to the α- and β-carbons of the vinylidene moiety, respectively. The C_β-hydrogen atom displays a doublet centered at 5.04 ppm (1H, J(HP) = 4.0 Hz). Finally, the resonances of Tp and pn are in the expected ranges. The overall octahedral structure of **7** (in form of its solvate **7**·CH_2Cl_2), as shown in Figure 4, is very similar to those of **3**, **4**, **5**, and **6**. However, the two Ru−N(Tp) bond distances *cis* to the vinylidene moiety are significantly shorter (Ru−N(2) = 2.146(4) Å, Ru−N(4) = 2.076(4) Å) than the one *trans* to vinylidene (Ru−N(6) = 2.209(4) Å). The Ru−N(pn) and Ru−P bond lengths are 2.214(4) and 2.309(2) Å), respectively. The Ru−C(26) bond distance is 1.821(5) Å, comparable to the 1.820 (5) Å of the previously reported vinylidene complex [RuTp(tmeda)-(═C═CHPh)]$^+$ [1] but slightly shorter than in others.[22] The Ru═C═C group is virtually linear (Ru−C(26)−C(27) angle = 169.6(4)°). The C(26)−C(27) bond distance is 1.287(2) Å, corresponding to a bond order between 2 and 3.

The cationc complex [RuTp(pn)(η^1-N$_2$)]$^+$ (**8**) exhibits, in the IR spectrum, the ν(N≡N) frequency at 2182 cm^{-1} which is one of the highest values ever recorded for a ruthenium dinitrogen complex, exceeded only by 2203 cm^{-1} measured for Ru(TMP)-(N$_2$)$_2$ (TMP = 5,10,15,20-tetramesitylporphyrin),[23] while typical values are in the range 2103−2167 cm^{-1} (Table 3).[23−30] A

(19) Gould, R. O.; Sime, W. J.; Stephenson, T. A. *J. Chem. Soc., Dalton Trans.* **1978**, 76.
(20) Esteruelas, M. A.; Lahoz, F. J.; Lopez, A. M.; Onate, E.; Oro, L. A. *Organometallics* **1994**, *13*, 1669.
(21) Lindsay, A. J.; Wilkinson, G.; Motevalli, M.; Hursthouse, M. B. *J. Chem. Soc., Dalton Trans.* **1985**, 2321.
(22) Bruce, M. I. *Chem. Rev.* **1991**, *91*, 197.
(23) Camenzind, M. J.; James, B. R.; Dolphin, D. *J. Chem. Soc., Chem. Commun.* **1986**, 1137.
(24) Camenzind, M. J.; James, B. R.; Dolphin, D.; Sparapany J. W.; Ibers, J. A. *Inorg. Chem.* **1988**, *27*, 3054.
(25) Davis B. R.; Ibers, J. A. *Inorg. Chem.* **1970**, *9*, 2768.
(26) Jia, G.; Meek, D. W.; Gallucci, J. C. *Inorg. Chem.* **1991**, 30, 403.
(27) Chaudret, B.; Devillers, J.; Poilblanc, R. *Organometallics* **1985** *4*, 1727.

Table 4. Selected IR Spectroscopic and X-ray Crystallographic Data for the Ruthenium η^1-Dinitrogen Complexes

compound	ν(N≡N), cm^{-1}	Ru−N, Å	N≡N, Å	∠Ru−N−N, deg	ref
$[RuTp(pn)(N_2)]^+$ (**8**)	2182	1.943(4)	1.097(5)	174.6(4)	this work
$[Ru(en)(N_3)(N_2)]^+$ [a]	2103	1.894(9)	1.106(11)	179.3(9)	25
$RuH_2(Cyttp)(N_2)$ [b]	2100	2.005(6)	1.093(8)	175.4(7)	26
$Ru(TMP)(THF)(N_2)$ [c]	2110	1.822(13)	1.074(16)	177.6(16)	23, 24
$Ru_2H_4(PPh_3)_4(N_2)$	2140	2.01(4)	1.08(4)	171(5)	27

[a] en = $H_2NCH_2CH_2NH_2$. [b] Cyttp = $PhP(CH_2CH_2CH_2PCy_2)_2$. [c] TMP = 5,10,15,20-tetramesitylporphyrin.

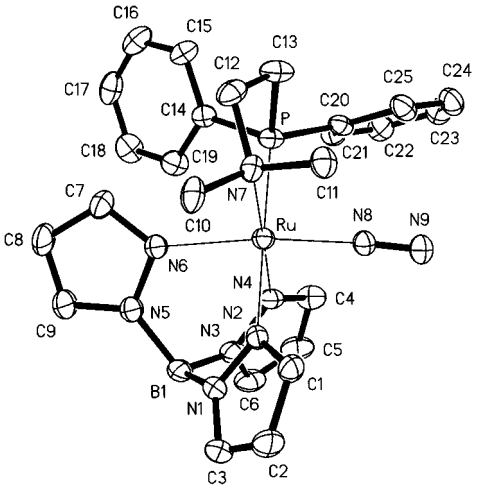

Figure 5. Structural view of $[RuTp(pn)(\eta^1\text{-}N_2)]BPh_4 \cdot CH_2Cl_2$ (**8**·CH_2Cl_2) (BPh_4^- and CH_2Cl_2 omitted for clarity).

structural view of **8** is shown in Figure 5. The geometry of the coordination sphere is nearly octahedral. The Ru−N(8) bond distance is 1.943(4) Å and is thus within the range 1.822−2.010 Å found for other ruthenium dinitrogen complexes (Table 4). Likewise, the N≡N triple bond distance is 1.097(5) Å comparable to others (see references in Table 4) but within experimental errors just that in free N_2 (1.0975 Å).[31] By this criterion the present complex is sometimes termed a van der Waals complex.[32] Notwithstanding this, the insensitivity of the N−N bond of the dinitrogen ligand to relative strong bond formation between a metal and the dinitrogen molecule appears to be not fully understood. It has been suggested that "σ donation" is more important for the formation of the metal−nitrogen bond than "π back-donation", which mainly contributes to the weakening of the nitrogen−nitrogen bond.[33]

Summing up, the RuTp(pn)L complexes can be described as tetragonally distorted octahedra. The nature of L has only a marginal effect on the dimensions of the rigid $[RuTp(pn)]^+$ fragment, irrespective of the length (i.e., strength) of the Ru-L bond ranging from 1.821 (vinylidene) to 2.190 Å (H_2O). The molecular geometry is maintained even in the case of quite different co-ligands such as in the ruthenatetraborane $[RuTp(PPh_3)(B_3H_8)]$.[34] The most notable deviation from octahedral geometry is exhibited by the Tp nitrogen trans to L (trans effect). In order to better understand the nature of the bonds, we have carried out EHMO calculations. In particular, we would like to explain (i) the order of complex stabilities depending on the ligand L and (ii) the relatively strong dinitrogen complexation affecting the $RuTp(pn)^+$ fragment similarly to vinylidene or CO but with the N−N bond length remaining unaltered.

EHMO Calculations. The virtually regular square pyramide of the $[RuTp(pn)]^+$ fragment (C_{4c}) is held together by mainly σ bonds without any significant participation of the d(π) AOs (d_{xy}, d_{xz}, d_{yz}) of Ru. The MO scheme of this fragment is very similar to that of $[RuTp(tmeda)]^+$ displayed before.[1] A small difference in the d splittings originates from the higher electronegativity of N compared to P (Table 5). The highest d(σ*) MO of Ru (Ψ_{Ru} 1, or "classical" $d_{x^2-y^2}$) is responsible for the square-pyramidal geometry of the $[RuTp(pn)]^+$ fragment remaining invariant with the coordination of the sixth ligand trans to the apical N. The other d(σ*) MO (Ψ_{Ru} 2, or "classical" d_{z^2}, LUMO) is open faced and strongly localized. This MO is responsible for the appreciable σ affinity of the vacant site capable of conducting inductive effects through the N(apex)−Ru−L line. As seen in Table 2, the Ru−X−Y angles (where X is the donor atom of L and Y is its neighbour atom) are deviating from 180°. However, these deviations are within the flat energy minimum positioned at 180 ± 10° in the Walsh diagram for all L's, except for acetone, as displayed by computer simulations of the complex geometries implying the participation of only s (in the case of N_2) and/or sp AOs of L, without notable sp^2 contribution. Therefore, the deviations from linearity are to be considered as packing force effects. This is also valid for acetone despite the small angle Ru−O−C of 137.1° which could be interpreted in terms of a rehybridization from sp to sp^2. However, the Walsh diagram in this case shows a very broad minimum ranging from 140 to 170°. Thus, instead of an sp^2 hybridization, the interaction of both the free sp and p electron pairs of the O atom with d(σ) and d(π) Ru, respectively, is indicated.

Of the Ru orbitals, Ψ_{Ru} 2 is most strongly affected by coordination of L as seen from Table 5. The energy level of this σ* MO can in fact be taken as an indicator of the σ donor strength of L varying inversely to the electronegativity of the donor atoms C(sp) (2.99) > N(sp) (3.68) > O(sp) (4.42), where the Mulliken electronegativities are given in parentheses.[35] From this point of view, the effects of coordinating N_2 and CO or CH_3CN on Ru could well be expected to be similar in magnitude.

Let us now briefly discuss the π MOs of the complexes. Ψ_{Ru} 3, or "classical" d_{xy}, is the HOMO of the $[RuTp(pn)]^+$ fragment. Since it is located in the plane of the pyramid base, it does not interact with L. Whether or not it remains the HOMO in the octahedral configuration depends on the strength of π overlap between L and Ψ_{Ru} 4 and Ψ_{Ru} 5 and the other co-ligands (see Table 5). The two other d(π) MOs (Ψ_{Ru} 4 or "classical" d_{xz} and Ψ_{Ru} 5 or "classical" d_{yz}) are responsible for the π affinity of $RuTp(pn)^+$ and can act as either π donors or π acceptors depending on the nature of L and the electronic population on the two MOs.

It should be remarked here that the Tp ligand itself has been

(28) Knoth, W. H. *J. Am. Chem. Soc.* **1972**, *94*, 104.
(29) Bancroft, G. M.; Mays, M. J.; Prater, B. E.; Stefanini, F. P. *J. Chem. Soc. A* **1970**, 2046.
(30) Allen, A. D.; Bottomley, F.; Harris, R. O.; Reinsalu, V. P.; Senoff, C. V. *J. Am. Chem. Soc.* **1967**, *89*, 5595.
(31) Wilkinson, P. G.; Houk, N. B. *J. Chem. Phys.* **1956**, *24*, 128.
(32) Brock, L. R.; Duncan, M. A. *J. Chem.Phys.* **1995**, *102*, 9498.
(33) Yamabe, T.; Hori, K.; Minato, T.; Fukui, K. *Inorg. Chem.* **1980**, *19*, 2154.
(34) Burns, I. D.; Hill, A. F.; Williams, D. J. *Inorg. Chem.* **1996**, *35*, 2685
(35) Bratsch, S. G. *J. Chem. Educ.* **1988**, *65*, 34

Table 5. Relevant MO Energy Levels (eV) of the $[RuTp(pn)L]^+$ Fragment as a Function of L

	E, eV						
	$\Psi_{Ru}1$ σ^*,$d_{x^2-y^2}$	$\Psi_{Ru}2$ σ^*, d_{z^2}	$\Psi_{Ru}3$ π, d_{xy}	$\Psi_{Ru}4$ π, d_{xz}	$\Psi_{Ru}5$ π, d_{yz}	E_{stab},[c] eV	χ[d]
$[RuTp(tmeda)]^+$ [a]	−7.10	−9.77	−11.36	−11.55	−11.74		
$[RuTp(pn)]^+$ [a]	−6.52	−9.84	−11.37	−11.52	−11.74		
$[RuTp(pn)(=C=CHPh)]^+$	−6.82	−4.48	−11.39	−11.24	−9.10	3.94	
$[RuTp(pn)(CO)]^+$	−6.76	−4.47	−11.38	−11.67	−8.01	4.09	6.1
$[RuTp(pn)(N_2)]^+$	−6.85	−5.29	−11.36	−11.54	−11.85	3.03	6.5
$[RuTp(pn)(CH_3CN)]^+$	−6.73	−5.43	−11.34	−11.26	−11.61	1.35	4.7
$[RuTp(pn)(acetone)]^+$	−6.21	−7.37	−11.35	−11.29	−11.61	0.32	4.1
$[RuTp(pn)(H_2O)]^+$	−6.36	−7.77	−11.36	−11.30	−11.67	0.48	3.1
$RuTp(pn)(CF_3SO_3)$[b]	−6.31	−7.62	−11.36	−11.30	−11.64	0.03	

[a] Fragment. [b] Based on the structure obtained from geometry optimization. [c] E_{stab} is the stabilization energy given by the difference between E_{tot} of the complex and the sum of E_{tot} of the fragments and E_{tot} of L at 0 K. [d] Electronegativity according to Pearson.[43]

classified as a good π-donor.[36] This property, however, becomes noticeable only in the presence of appropriate, i.e, π-accepting, co-ligands such as CO. In addition, such a $\pi-\pi$ resonance between the ligands through the metal center is particularly effective in the case of C_{3v} symmetry where all three π orbitals of the metal are equally participating in the metal−ligand bondings as in $TpMo(CO)_3$.[36] In the case with pn as the co-ligand, however, the interactions between d(π) and π or π* of the pyrazolyl rings of the Tp ligand are insignificant.

The $[RuTp(pn)]^+$ fragment has a high affinity to coordinate a sixth ligand trans to N(6) of Tp provided it is π overlapping. Of the ligands considered, vinylidene or CO are the most strongly bound because of its high π acidity. According to the orbital interaction diagram shown in Figure 5, the bonding between Ru and N_2 is due to both d(σ)−sp and d(π)−p interactions.

The data in Table 5 reveal that none of the ligands, apart from vinylidene or CO, is particularly $\pi-\pi$ interacting with $[RuTp(pn)]^+$. That vinylidene is a strong π acceptor is seen by the pronounced decrease in the energy of Ψ_{Ru} 5 from −11.74 to −9.10 eV. The orbital interaction diagram is similar to that depicted before[1] and is therefore omitted here. Thus the main contribution to bonding is the $\pi-\pi$ interaction between the empty p orbital (LUMO) of vinylidene taking over electron density from the π AOs of Ru owing to which the formal oxidation state of Ru should be considered as +IV(charge transfer character of complex). The interaction brings about a notable destabilization of the Ru−N(apex) bond as is also visualized by the crystal structure. This trans effect is further increased by the $\sigma-\sigma$ interaction between the occupied sp (HOMO) of vinylidene and the d(σ)* orbitals of Ru (Ψ_{Ru} 3). In addition, the strong $Ru-C_\alpha$ bond originating from the p(vinylidene)−d(π) (Ru) interaction is strengthened by the participation of the empty π* orbital of vinylidene. In the CO case this $\pi-\pi$ interaction is smaller with minor charge transfer from Ru to CO, although the effect of the CO ligand is comparable to that of vinylidene. Incidentally, it may be worth noting that in the case of N_2 complexation both the Ψ_{Ru} 4 and Ψ_{Ru} 5 orbitals are slightly raised relative to parent $[RuTp(pn)]^+$, instead of lowered as in the other cases, and this may be viewed as pointing to some π donor action of N_2.

Dinitrogen is a very weak base and does not interact even with the strongest acids such as H^+. Its proton affinity is even less than that of, e.g., methane.[37] In contrast, the N_2 affinity to low valence d metal cations such as Ni^+, Co^+, Cr^+, or Fe^+, though weakly acidic, is large with the bond dissociation energies decreasing in the row from 26.5 to 10.7 kcal/mol.[38]

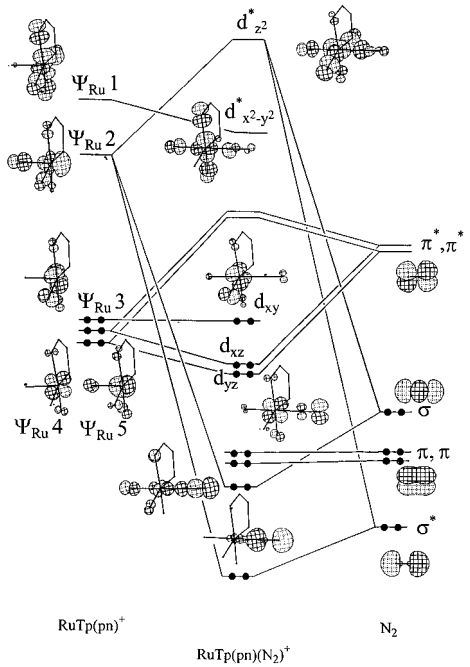

Figure 6. Orbital interaction diagram for the formation of $[RuTp(pn)(\eta^1\text{-}N_2)]^+$ (**8**) ($\sigma^* = 2\sigma_u$, $\sigma = 3\sigma_g$; $2\sigma_g$ and $3\sigma_u$ is omitted).

According to the orbital interaction diagram shown in Figure 6, the bonding between Ru and dinitrogen is due to both d(σ)−sp and d(π)−π interactions, while both Ψ_{Ru} 1 und Ψ_{Ru} 3 MOs are not involved. The highest overlap population is between Ψ_{Ru} 2 and two high σ and σ* MO's of N_2 (23 and 9%). The lowering of the energy of Ψ_{Ru} 2 from −9.84 eV in $[RuTp(pn)]^+$ to −5.29 eV in $[RuTp(pn)(\eta^1\text{-}N_2)]^+$ (Table 5), pointing to the notable σ donor strengh of N_2, is responsible for the considerable exothermicity of such type of reaction which has recently been reported to be as high as about 18 kJ/mol for a similar end-on N_2 complexation to a coordinatively unsaturated Fe complex.[39] Notice that the equilibrium constant $K_{eq} = 2.1$ given in that paper for the reversible dinitrogen dissociation is an effective one, including the solubility of N_2 in acetone amounting to about 7.4 mmol L^{-1} at 298 K.[40] Thus, the true stability constant (as the reverse of the dissociation constant) might be on the order of 65 L mol^{-1} demonstrating again that N_2 is a pretty good donor for the complex type under consideration. On the basis of the present results in combination

(36) Curtis, M. D.; Shiu, K.; Butler, W. M.; Huffman, J. C. *J. Am. Chem. Soc*. **1986**, *108*, 3335.
(37) Bazhenova, T. A.; Shilov, A. E. *Coord. Chem. Rev*. **1995**, *144*, 169
(38) Heinemann, C.; Schwarz, J.; Schwarz, H. *J. Phys. Chem*. **1996**, *100*, 6088
(39) Leal, A. J.; Tenorio, M. J.; Puerta M. C.; Valerga, P. *Organometallics* **1995**, *14*, 3839
(40) Kretschmer, C. B.; Nowakowska, J.; Wiebe, R. *Ind. Eng. Chem.* **1946**, *38*, 506.

Table 6. Charateristic Properties of $[RuTp(pn)]^+$ Fragment as a Function of L

	=C=CHPh	CO	N_2	CH_3CN	acetone	H_2O	$CF_3SO_3^-$	without L
$Ru-N_{(trans\ to\ L)}$, Å	2.209	2.175	2.102	2.093	2.075	2.071		
E_{stab}, eV	3.938	4.09	3.034	1.351	0.32	0.476	0.030	0
χ		6.1	6.7	4.7	4.1	3.1		
$E(\Psi_{Ru}2, \sigma^*, d_{z^2})$, eV	−4.481	−4.896	−5.289	−5.426	−7.374	−7.767	−7.667	−9.838

with a previous work on similar cyanide complexes[41] we are led to rationalize the absence of N−N bond changes despite strong N_2 end-on complexation in terms of a superposition of two effects counteracting one another: (i) The involvement of σ^* MOs of dinitrogen in σ bonding with Ru (Figure 6) reduces the antibonding character, thereby provoking a decrease in the N−N bond length as has been shown in the case of ruthenium cyanide complexes.[41] (ii) π back-bonding weakens the N−N bond. The small overlap population between both Ψ_{Ru} 4 and Ψ_{Ru} 5 and the π^* MOs of N_2 (6% each) testifies to the minor importance of back-donation in the present case.

Conclusions

Experimental material is presented that allows one to analyze inorganic dinitrogen ligation in solution not merely as a stand-alone phenomenon but to put it in perspective to other complex formations. Both the EHMO stabilization energies, reflecting the energy gained by complex formation, and the energies of $\Psi_{Ru}2$ increase in the order $CF_3SO_3^- < H_2O \approx$ acetone $< CH_3CN < N_2 < CO \approx$ vinylidene (Table 6). This order is paralleled by the crystallographic Ru−N(trans to L) bond lengths (trans influence) comprising the whole range of Ru−N bond lengths found in Ru−Tp complexes.[42] Since $\Psi_{Ru}2$ is responsible for the inductive effects mediated through the N(apex)−Ru−L line, the rough trend with the ligand electronegativity χ is comprehensible (Table 5).[43] The strong bond formation between ruthenium and the dinitrogen ligand is thus substantiated.

Another comment concerns the N−N bond length of ligated dinitrogen which in present $[RuTp(pn)(\eta^1\text{-}N_2)]^+$ just equals that in free N_2. It has often been noted that end-on ligation of N_2 is little felt in the N−N bond length. What is notoriously looked forward to eagerly is bond weakening according to the back-donation picture. However, there are also at least two cases known[24,37] where even some bond strengthening seems to have taken place, although these data may be dismissed as lying within the experimental uncertainties. The possibility of N−N bond shortening may not in principle be ruled out since in dinitrogen ligation a decrease in the antibonding character of a σ^* MO ($2\sigma_u$) is involved effecting some σ-bond strengthening (see the interaction between $\Psi_{Ru}2$ of $[RuTp(pn)]^+$ and σ^* of N_2 in Figure 6). It is this kind of interaction that causes C−N bond shortening upon complexation of (isoelectronic) cyanide.[41] It is indeed appealing to rationalize the invariance of the N−N bond length, despite strong N_2 fixation, as due to a delicate compensatory influence of σ-bond strengthening and π-bond weakening in the dinitrogen molecule.

Acknowledgment. Financial support by the "Jubiläumsfond der Österreichischen Nationalbank" is gratefully acknowledged (Project 5305).

Supporting Information Available: Listings of atomic coordinates, equivalent isotropic displacement parameters, anisotropic displacement parameters, complete bond lengths and angles, and least-squares planes for complexes **3**·$^1/_2CH_2Cl_2$, **4**, **6**, **7**·CH_2Cl_2, and **8**·CH_2Cl_2 (66 pages). Ordering information is given on any current masthead page.

IC961128D

(41) Sapunov, V. N.; Mereiter, K.; Schmid, R.; Kirchner, K. *J Organomet. Chem.* **1997**, in press

(42) (a) Sun, N.-Y.; Simpson, S. J. *J. Organomet. Chem.* **1992**, *434*, 341. (b) Alcock, N. W.; Burns, I. D.; Claire, K. S.; Hill, A. F. *Inorg. Chem.* **1992**, *31*, 2906. (c) Alcock, N. W.; Hill, A. F.; Melling, R. B. *Organometallics* **1991**, *10*, 3898. (d) Hill, A. F.; *J. Organomet. Chem.* **1990**, *395*, C35. (e) Steyn, M. M. deV.; Singleton, E.; Hietkamp, S.; Liles, D. C. *J. Chem. Soc., Dalton Trans.* **1990**, 2991. (f) McNair, A. M.; Boyd, D. C.; Mann, K. R. *Organometallics* **1986**, *5*, 303.

(43) Pearson, G. *Inorg. Chem.* **1988**, *27*, 734.